J|A|C|S
JOURNAL OF THE AMERICAN CHEMICAL SOCIETY
Article
pubs.acs.org/JACS

Impact of Metal and Anion Substitutions on the Hydrogen Storage Properties of M-BTT Metal–Organic Frameworks

Kenji Sumida,[†,◆] David Stück,[†,◆] Lorenzo Mino,[‡] Jeng-Da Chai,[†,⊥] Eric D. Bloch,[†] Olena Zavorotynska,[‡,∇] Leslie J. Murray,[†,#] Mircea Dincă,[†,○] Sachin Chavan,[‡] Silvia Bordiga,*[‡] Martin Head-Gordon,*[†,‖] and Jeffrey R. Long*[†,§]

[†]Department of Chemistry, University of California, Berkeley, California 94720, United States
[‡]Department of Chemistry, NIS Centre of Excellence and INSTM, University of Torino, Via Quarello, 11 I-10135 Torino, Italy
[‖]Chemical Sciences Division and [§]Materials Sciences Division, Lawrence Berkeley National Laboratory, Berkeley, California 94720, United States

Ⓢ *Supporting Information*

ABSTRACT: Microporous metal–organic frameworks are a class of materials being vigorously investigated for mobile hydrogen storage applications. For high-pressure storage at ambient temperatures, the $M_3[(M_4Cl)_3(BTT)_8]_2$ (M-BTT; BTT^{3-} = 1,3,5-benzenetristetrazolate) series of frameworks are of particular interest due to the high density of exposed metal cation sites on the pore surface. These sites give enhanced zero-coverage isosteric heats of adsorption (Q_{st}) approaching the optimal value for ambient storage applications. However, the Q_{st} parameter provides only a limited insight into the thermodynamics of the individual adsorption sites, the tuning of which is paramount for optimizing the storage performance. Here, we begin by performing variable-temperature infrared spectroscopy studies of Mn-, Fe-, and Cu-BTT, allowing the thermodynamics of H_2 adsorption to be probed experimentally. This is complemented by a detailed DFT study, in which molecular fragments representing the metal clusters within the extended solid are simulated to obtain a more thorough description of the structural and thermodynamic aspects of H_2 adsorption at the strongest binding sites. Then, the effect of substitutions at the metal cluster (metal ion and anion within the tetranuclear cluster) is discussed, showing that the configuration of this unit indeed plays an important role in determining the affinity of the framework toward H_2. Interestingly, the theoretical study has identified that the Zn-based analogs would be expected to facilitate enhanced adsorption profiles over the compounds synthesized experimentally, highlighting the importance of a combined experimental and theoretical approach to the design and synthesis of new frameworks for H_2 storage applications.

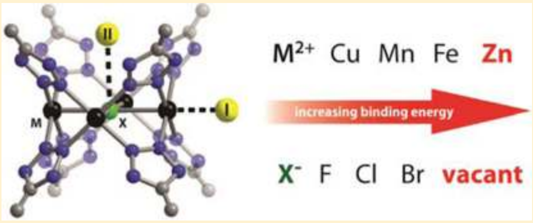

■ INTRODUCTION

The widespread deployment of carbon-neutral energy sources for use in mobile applications is of paramount importance due to the increasing atmospheric levels of CO_2 resulting from the combustion of fossil fuels.[1] As a result of its high-energy content, clean combustion, and potential renewability, hydrogen is one of the leading candidates to supplant carbon-based fuels, although its high fugacity presents a crucial challenge in terms of its safe and efficient storage.[2] The U.S. Department of Energy (DoE) system performance targets for mobile hydrogen storage systems,[3] which specify minimum performance requirements for the storage capacity, operating temperature, system cost, kinetics of delivery and refueling, and lifetime of the storage system, are yet to be satisfied by a single storage solution. For example, although the compression of hydrogen within insulated pressure tanks represents the simplest method for its storage,[4] the cooling systems used in these configurations contribute a significant additional mass to the vehicle as a whole and also require the addition of coolant in order to achieve sufficient hydrogen storage densities. This has spurred interest in a variety of other modes of hydrogen storage, including chemisorptive systems, such as metal hydrides,[5] and physisorptive storage within high-surface area porous materials, such as metal–organic frameworks.[6]

The design of an efficient adsorbent-based system requires careful consideration of the thermodynamics of H_2 adsorption, namely the enthalpy (ΔH_{ads}) and entropy (ΔS_{ads}) change associated with the adsorption event. As such, most of the efforts to date in the context of materials design have been targeted toward the optimization of ΔH_{ads} through control of the chemical and physical nature of the adsorbing surface. Assuming a constant ΔS_{ads} term of $-8R$, the optimal ΔH_{ads} across the entire adsorption range for an adsorbent operating at 298 K between 100 and 1.5 bar is found to be −13.6 kJ/mol.[7] However, experimental evidence stemming from H_2 adsorption studies within zeolite-based systems has suggested that the value for ΔS_{ads} is correlated to the magnitude of ΔH_{ads}, wherein

Received: October 15, 2012
Published: December 17, 2012

dx.doi.org/10.1021/ja310173e | *J. Am. Chem. Soc.* 2013, 135, 1083–1091

strong adsorbent-H_2 interactions impose a more rigid spatial ordering of the H_2 molecules, resulting in a more negative ΔS_{ads} term.[8] Inclusion of this enthalpy−entropy correlation leads to a larger magnitude of the optimal ΔH_{ads} value, such that it lies in the range of −20 to −25 kJ/mol for an adsorbent operating under the same conditions. Regardless, the precise control over the thermodynamics of the adsorption process is crucial in the design of new materials that offer enhanced storage performance compared to existing systems.

Metal−organic frameworks[9] have received significant recent attention as adsorbents for use in hydrogen storage systems due to their high permanent porosity and the ability for the chemical features of the pore surfaces to be finely tuned.[6] Indeed, in a number of the highest surface area materials, adsorption capacities exceeding the gravimetric and volumetric storage densities specified by the 2017 DoE targets[3] of 5.5 wt % and 40 g/L, respectively, have been observed at cryogenic temperatures.[9h,10] For example, $Zn_4O(BDC)_3$ (MOF-5; BDC^{2-} = 1,4-benzenedicarboxylate) offers the best overall cryogenic H_2 storage performance within a metal−organic framework to date, exhibiting a total volumetric adsorption capacity of 66 g/L (10 wt %) at 77 K and 100 bar.[10l] However, as a result of the weak affinity ($\Delta H_{ads} \approx -5$ to −7 kJ/mol) of H_2 for the framework surface, the adsorption capacity is greatly diminished at ambient temperatures. Indeed, the volumetric storage capacity of just 10 g/L at 298 K and 100 bar represents only a marginal enhancement in the storage density over compressed H_2 at the same pressures. Thus, increasing the affinity of the surfaces of metal−organic frameworks toward H_2 is a crucial endeavor if enhanced capacities are to be achieved at ambient temperatures.

One of the primary strategies that have been explored to date for increasing the ΔH_{ads} of H_2 adsorption within metal−organic frameworks is the preparation of materials furnished with exposed metal cation sites on the surfaces of the pores.[6a,10o,11] These metal centers act as charge-dense binding sites that polarize the H_2 molecule, creating a dipole−induced dipole interaction that is stronger than the dispersion-type interactions that predominate within most porous materials. Indeed, a site-specific ΔH_{ads} as high as −13.5 kJ/mol has been observed via variable-temperature infrared spectroscopy for H_2 adsorbed within the framework Ni_2(dobdc) (Ni-MOF-74, CPO-27-Ni; $dobdc^{4-}$ = 2,5-dioxido-1,4-benzenedicarboxylate), which features a high density of exposed Ni^{2+} sites following activation.[12] Moreover, systematic evaluation of the thermodynamics of H_2 adsorption within the M_2(dobdc) series (M = Mg, Mn, Co, Ni, Zn) has revealed that the identity of the metal center and its associated positive charge density has a considerable influence on the enthalpy of adsorption.[11j] In this regard, further increases in the binding enthalpy through control of the charge density at the metal centers embedded within metal−organic frameworks via ligand design (for example, through the use of less-donating coordinating groups or the installation of electron-withdrawing groups on the ligand backbone) or the use of metal centers with smaller radii (including the use of tri- or tetravalent metal ions), coupled with the discovery of new structure types featuring a high density of exposed metal sites, is a particularly promising strategy for boosting the storage capacity.

In addition to this experimental strategy, the use of electronic structure calculations in a complementary manner to the experimental synthesis is a further means for gaining a greater insight into the factors affecting the H_2 storage performance and, perhaps of equal significance, a pathway to identifying new target materials offering enhanced storage densities. Here, density functional theory (DFT) is emerging as an invaluable tool for acquiring accurate descriptions of increasingly large chemical systems, although the parametrized nature of DFT makes understanding the limits of the numerous functionals vital in assuring that the results obtained are of a high reliability.[13,14] Indeed, the shortcomings of many functionals include the inability to describe dispersion interactions and the introduction of a self-interaction error, wherein an electron artificially repels itself.[15] Attempts to correct these problems involve the inclusion of explicit dispersion corrections in the form of −D and other methods[16,17] and the method of range-separated hybrids which include an amount of Hartree−Fock (HF) exchange that increases with distance to decrease the length scale at which the self-interaction error can persist. With such issues in mind, the hybrid, range-separated, dispersion-corrected density functional ωB97X-D provides a high accuracy for thermochemistry as well as weak intramolecular interactions,[18,19] and is expected to serve as an ideal platform for the study of H_2 adsorption within metal-organic frameworks.

Herein, we report a combined theoretical and experimental study of the adsorption of H_2 within the M-BTT (Figure 1; BTT^{3-} = 1,3,5-benzenetristetrazolate) structure type. We have previously reported the synthesis, characterization, and bulk H_2 adsorption properties of the Mn-,[20] Fe-,[21] and Cu-based analogs,[22] although many aspects related to the thermodynamics of adsorption within these compounds have remained unexplored, owing to the limited information that can be obtained from the adsorption isotherms.[23] Here, through the use of both theoretical DFT calculations and experimental variable-temperature infrared (VTIR) spectra, a complete description of the thermodynamics of H_2 adsorption within this series of frameworks is obtained. Furthermore, the success of the DFT functional ωB97X-D in describing the experimentally examined systems has allowed the calculations to be extended to a hypothetical Zn-based analog, which is demonstrated as being likely to afford enhanced ΔH_{ads} values compared to the other members of the series. As such, the results demonstrate the value of DFT calculations in providing a better understanding of the H_2 adsorption within metal−organic frameworks and their potential to assist in the identification of new target materials of interest for H_2 storage at ambient temperatures.

EXPERIMENTAL SECTION

All reagents and solvents were acquired from commercial vendors and used without further purification. The H_3BTT ligand and the as-synthesized forms of the metal−organic frameworks Mn-, Fe-, and Cu-BTT used in the experimental studies were prepared according to the literature procedures.[20−22] The phase purity of the samples was confirmed by powder X-ray diffraction. In a typical preparation, the as-synthesized forms of the frameworks were washed several times in hot DMF, followed by solvent exchange in MeOH via Soxhlet extraction for at least 3 days. The activation procedures were carried out as reported previously, and the desolvated materials were stored in a glovebox under a nitrogen atmosphere. The isosteric heat of adsorption plots for the three frameworks was generated by first fitting the 77 and 87 K H_2 adsorption isotherms using the dual-site Langmuir model, followed by application of the Clausius−Clapeyron equation in a manner described elsewhere.[24] Owing to the very steep initial portion of the H_2 isotherm for Fe-BTT recorded at 77 K, the lowest-pressure data (up to a loading of 1 mmol/g, see Figure S7) were fit with a second dual-site Langmuir function to ensure the highest possible accuracy of the isosteric heat of adsorption down to

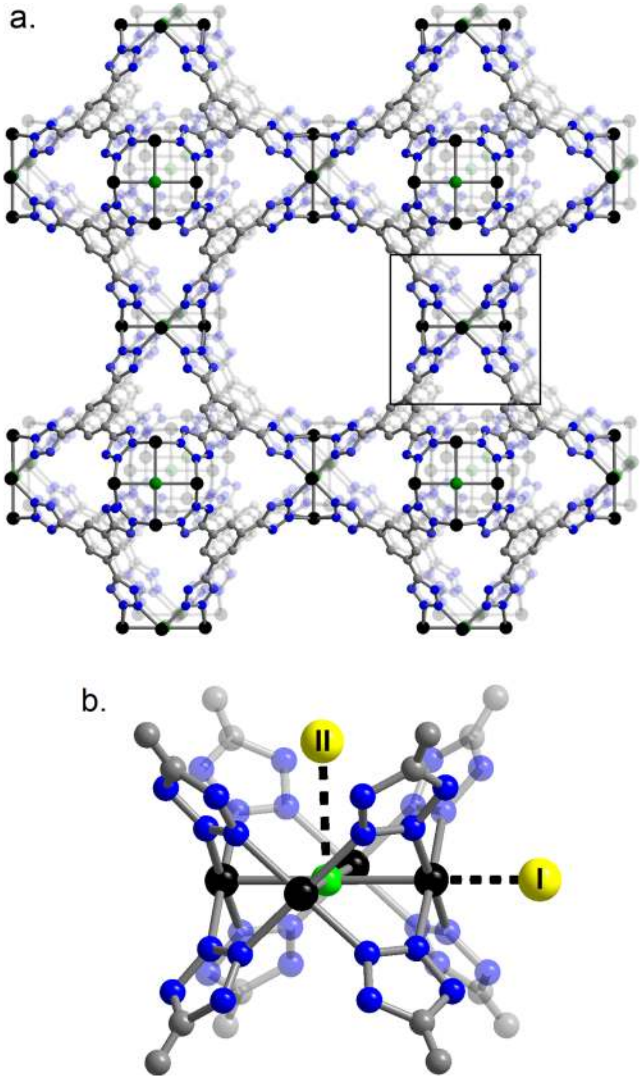

Figure 1. (a) A portion of the structure of the M-BTT (M = Mn, Fe, Cu) structure type. Black, green, gray, and blue spheres represent M, Cl, C, and N atoms, respectively. Solvent molecules, H atoms, and charge-balancing cations are omitted for clarity. (b) An expanded view of the region enclosed by the black outline in the upper figure showing the two predominant D_2 binding sites as observed in powder neutron diffraction experiments, in which D_2 is accommodated in close proximity to the metal center (site I) and a bowl-shaped cavity directly above the chloride anion (site II). Note that the orientation of the D_2 molecules is not resolved at the temperatures probed.

the lowest coverages. All other isotherms could be adequately fit using a single dual-site Langmuir function.

Infrared Spectroscopy. For Cu- and Fe-BTT samples, the IR measurements were performed on a thin self-supported wafer, while for Mn-BTT, owing to the limited trasmittance of the material, the methanol-solvated powder was deposited on a KBr plate. An Oxford CCC 1204 cryostat was employed for the variable-temperature measurements. The samples were evacuated overnight at a residual pressure of less than 10^{-6} bar at 373 K, and final activation was performed under a high vacuum by heating to 423 K for 24 h. Infrared spectra were collected using a Bruker Equinox 55 FTIR spectrometer equipped with an MCT cryogenic detector with the sample compartment modified to accommodate the cryogenic head. The final spectra were obtained by taking the average of 512 interferograms, which were each recorded at a resolution of 1 cm^{-1}. The spectra for the H_2 adsorption were collected by dosing the sample with 50 mbar of H_2 at 260 K, followed by gradual cooling to 14 K while monitoring the gas-phase equilibrium pressure. Infrared spectra were collected at regular intervals between 260 and 14 K in order to ascertain the temperature dependence of the H_2 adsorption. The desorption behavior was probed by collection of spectra while progressively lowering the pressure of H_2 at 14 K (see Figures S1−3).

DFT Calculations. All calculations were performed with the Q-Chem electronic structure software.[25] Owing to the extended nature of the crystal structure, the computations were performed on a model compound $[M_4Cl(tz)_8]^-$ (M = Mn, Cu, Zn; tz^- = 5-*H*-tetrazolate), which represents a single $[M_4Cl]^{7+}$ square and its surrounding ligand environment as found in the M-BTT structure type, using the ωB97X-D functional.[13] A triple split-valence basis set with polarization (6-311G**)[26,27] was used with a small core Stuttgart−Born (SRSC) effective core potential to describe core electrons on the metal atoms.[28] Additionally, a large quadrature grid of size (99 590) was used to ensure high-quality results. An uncorrected hydrogen binding energy (HBE) was calculated using the expression:

$$\text{HBE} = (E_{\text{complex-H}_2} - nE_{\text{H}_2} - E_{\text{complex}})/n \qquad (1)$$

where $E_{\text{complex-H}_2}$, E_{H_2}, and E_{complex} represent the energies following binding of H_2 to the $[M_4Cl(tz)_8]^-$ complex, free H_2, and the bare molecular fragment, respectively, and n corresponds to the number of H_2 molecules introduced into the model system. The energy was then corrected for basis set superposition error (BSSE) using a standard counterpoise correction[29] as well as an estimate of the zero point energy. Zero point energy (ZPE) was accounted for by calculating H_2 frequency changes from the unbound to H_2-bound complex under the harmonic approximation. Frequencies were calculated using finite difference by running force calculations with H_2 molecules displaced by ±0.1 Å. Hydrogen vibrational frequencies were compared to a calculated free-hydrogen frequency by the same means, and these hydrogen shifts were then used to compare to experimental IR data.

■ RESULTS AND DISCUSSION

Structural Aspects. A portion of the structure of the M-BTT (M = Mn, Fe, Cu) framework[20−22] is presented in Figure 1a. The framework exhibits an expanded sodalite-type structure, in which truncated octahedral cages share square faces to form a microporous, cubic (3,8)-net. The square faces correspond to an $[M_4Cl]^{7+}$ unit, in which the axially bound solvent molecule at the metal centers can be removed to afford an exposed metal cation site. Here, the degree of desolvation that can be obtained experimentally is highly dependent on the metal. While the Cu-BTT compound can be fully desolvated, ∼70% and 30% of metal centers retain a MeOH molecule (originating from the solvent exchange procedure) within Mn- and Fe-BTT, respectively. Nevertheless, the Mn-BTT compound exhibits the highest BET surface area of the three compounds (2100 m^2/g), while the Fe-BTT (2010 m^2/g) and Cu-BTT (1710 m^2/g) feature slightly lower surface areas as a result of their relatively contracted unit cell volumes. This difference originates from the smaller ionic radii of the metal ions in the latter compounds (high-spin Mn^{2+}, 0.83 Å; Fe^{2+}, 0.78 Å; Cu^{2+}, 0.73 Å) and concomitantly shorter M−N and M−Cl bonds.

The predominant binding sites for H_2 within each of these materials have been probed via the collection of loading-dependent powder neutron diffraction data, revealing two main binding sites as shown in Figure 1b. For each of the three compounds, the highest-affinity binding site was adjacent to the exposed metal cation site (site I), while a secondary site associated with the bowl-shaped cavity formed by the chloride anion of the $[M_4Cl]^{7+}$ cluster and four tetrazolate units was also populated at low loadings (site II). The distance of site I from the metal site is found to depend on the identity of the metal, in which Fe-BTT exhibits the shortest site I distance from the metal center of 2.17 Å,[21] while Mn- and Cu-BTT display longer distances of 2.27 and 2.47 Å.[20,22] Here, the difference between Fe- and Mn-BTT can be rationalized by the smaller ionic radius of Fe^{2+} resulting in a greater degree of polarization of the adsorbates, giving stronger interactions that lead to a shorter distance from the surface. Meanwhile, Cu^{2+} features a distortion in the axial direction, resulting in a comparatively longer Cu^{2+}—H_2 distance. Interestingly, the distance between site II and the chloride anion is virtually unchanged across the series, suggesting that the affinity of the binding site toward H_2 is largely unaffected by the identity of the metal center.

Adsorption Data. The low-pressure H_2 adsorption isotherms for Mn-, Fe-, and Cu-BTT collected at 77 and 87 K are displayed in Figures S4−6. The capacities at 1.0 bar and 77 K are 2.1 , 2.3, and 2.3 wt % for Mn-, Fe-, and Cu-BTT, respectively. The fact that these capacities do not follow the trend observed for the BET surface areas of the frameworks suggests that the ability to desolvate the metal centers within Cu- and Fe-BTT to a greater degree than Mn-BTT plays a crucial role in determining the capacity at low pressures. Indeed, a plot of the isosteric heat of adsorption (Q_{st}) as a function of H_2 adsorbed (see Figure 2) obtained from fittings of the isotherm data to a dual-site Langmuir expression[24] reveals that the complete desolvation of Cu-BTT results in a virtually flat portion of the Q_{st} curve until around 2.0 mmol/g, which is a loading level in which approximately half of the Cu^{2+} sites are occupied. Note that the dual-site Langmuir model utilized here is more appropriate than the virial-type equation used previously for calculation of the Q_{st} function for materials featuring both strong and weak adsorption sites. For the Mn- and Fe-BTT frameworks, the respective initial Q_{st} values of −10.6 and −13.1 kJ/mol are greater in magnitude than for Cu-BTT (−9.8 kJ/mol), which is consistent with the trend in the ionic radii and the crystallographically observed distances of site I from the metal centers. However, the lower density of exposed metal cations in Mn- and Fe-BTT leads to a rapid decrease in the adsorption enthalpy with subsequent H_2 loading. As such, the Q_{st} value for Cu-BTT remains greater than for the other two frameworks until a loading approaching 7 mmol/g (1.4 wt %).

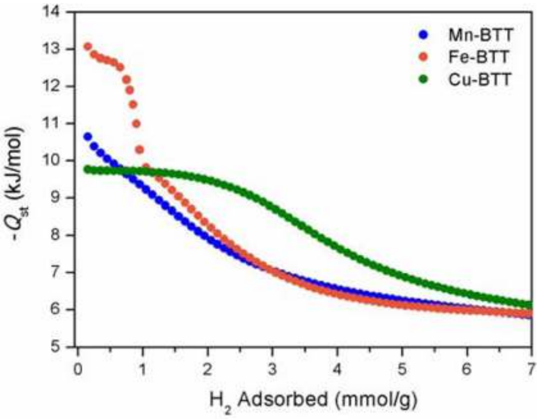

Figure 2. A plot of the isosteric heat of adsorption (Q_{st}) as a function of H_2 adsorbed as obtained using a dual-site Langmuir fitting to the adsorption isotherms.

Infrared Spectroscopy. Although the isosteric heat of adsorption plot displayed in Figure 2 gives an indication of the affinity of the pores of each of the frameworks toward H_2, it provides only a limited amount of site-specific information owing to the fact that it represents an average heat of adsorption over all of the available adsorption sites. Thus, here we probe the adsorption in more detail via variable-temperature infrared spectroscopy.[12,30] In a typical experiment, a known quantity (typically ca. 50 mbar) of H_2 was dosed onto the activated form of the framework at 260 K, and infrared spectra were collected at intervals of 5 K down to a final temperature of 14 K. The spectral features attributable to the adsorbed H_2 were obtained by taking difference spectra with the infrared spectrum of the activated material prior to H_2 loading. The spectra obtained for each of the three frameworks are now described in turn, followed by an evaluation of the site-specific ΔH_{ads} for H_2 binding at each of the metal centers.

Cu-BTT. The infrared spectra collected between 14 and 150 K for a sample of Cu-BTT dosed with H_2 are presented in Figure 3a. As the temperature is lowered from 150 K, a pair of absorption bands at 4058 and 4065 cm^{-1} are observed. These bands are shifted significantly lower in energy relative to the Raman-active gas phase (free) H−H stretching frequency (4161 cm^{-1}), which is indicative of some degree of polarization and activation of the H−H bond. The peak separation and their relative intensities are consistent with assignment of these peaks as an *ortho*−*para* pair corresponding to H_2 being bound at a single adsorption site within the framework. Since these bands are the only signals at the highest temperatures that can be ascribed to H_2 adsorption, they necessarily correspond to H_2 being bound at the strongest adsorption sites within the framework (site I). Below 120 K, a broader feature begins to evolve at 4120 cm^{-1}, which can be ascribed to a weaker adsorption site (site II), although their similar intensities and onset temperatures indicates that their adsorption enthalpies are comparable. This is in close agreement with loading-dependent powder neutron diffraction experiments previously performed on Cu-BTT, in which, at the lowest loadings, both sites I and II are occupied at similar occupancies. Note, however, that the crystallographic site multiplicity of site I is twice of that of site II, and the significantly greater intensity of the *ortho*−*para* pair at 4058 and 4065 cm^{-1} further supports its assignment as H_2 being bound to the Cu^{2+} sites.

Upon further cooling of the sample below 100 K, the evolution of additional features centered at 4085 and 4136 cm^{-1} is observed. These bands correspond to the significantly weaker interactions of H_2 molecules with the organic components of the framework. This is consistent with the crystallographic data, in which several additional binding sites in close proximity (<3.5 Å) to the ligands were observed at higher loadings, and with the isosteric heat of adsorption plot presented in Figure 2, which shows a dramatic decrease at higher loadings.

Mn-BTT. The infrared spectra for H_2 adsorbed within Mn-BTT collected between temperatures of 14 and 150 K are shown in Figure 3b. In comparison to the corresponding spectra for Cu-BTT presented in Figure 3a, the absorption band corresponding to H_2 bound at the exposed Mn^{2+} adsorption site (site I) is observed as a significantly broader feature centered at 4038 cm^{-1}. The shift of approximately −25 cm^{-1} relative to the H−H stretch observed for H_2 bound at the Cu^{2+} site within Cu-BTT is consistent with the greater polarization of H_2 bound to the Mn^{2+} cations. This is reflected in the closer approach of the D_2 molecules to Mn^{2+} (2.27 Å) compared to the Cu^{2+} distance (2.47 Å), as observed in the

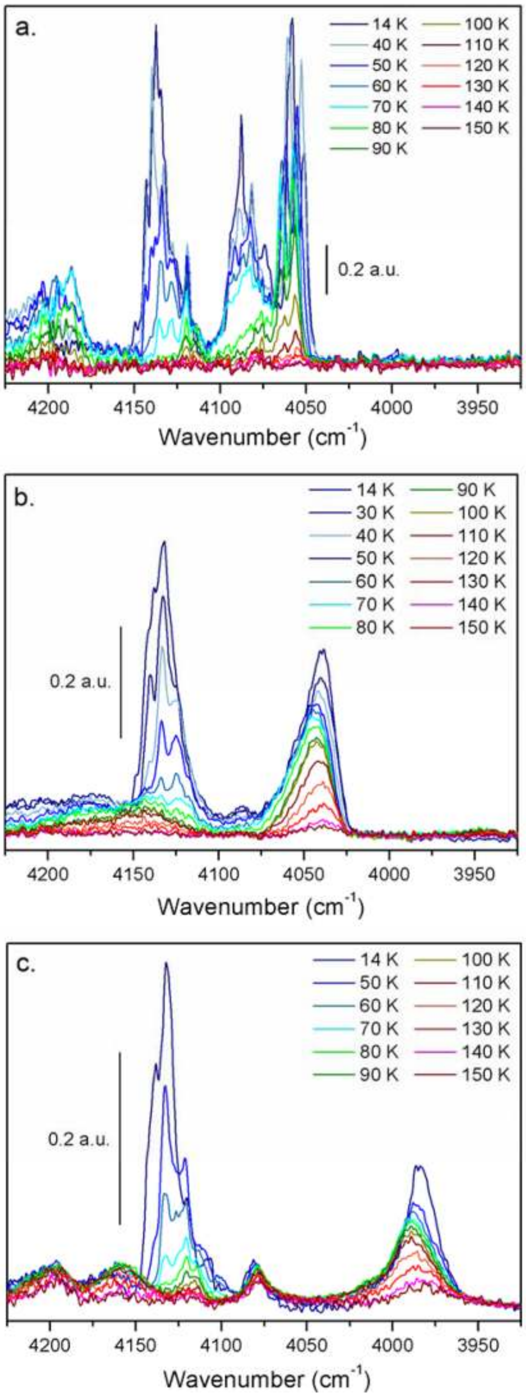

Figure 3. Selected variable-temperature infrared spectra for H_2 binding within (a) Cu-, (b) Mn-, and (c) Fe-BTT. The spectra represent an averaging of 512 interferograms collected at a resolution of 1 cm^{-1}.

powder neutron diffraction data as well as in the greater zero-coverage isosteric heat of adsorption compared to Cu-BTT. The broad nature of the absorption band is attributed to the presence of several binding environments for H_2 at the Mn^{2+} adsorption sites, owing to the partial solvation of the $[Mn_4Cl]^{7+}$ clusters throughout the material. Indeed, since just 30% of the Mn^{2+} within the structure can be desolvated experimentally, the number of exposed Mn^{2+} cations per tetranuclear unit is expected to reflect a statistical distribution between 0 and 4 exposed cation sites per cluster. The number of solvent molecules coordinated to the cluster not only dictates the number of H_2 molecules that can be accommodated per cluster but is also expected to have an influence on the charge density of the Mn^{2+} sites, which has a significant impact on the adsorption enthalpy. This is a contrast to the Cu-BTT material, in which all of the Cu^{2+} centers can be desolvated, where all binding sites at the metal cations are equivalent, giving a correspondingly sharper infrared absorption.

At temperatures below 100 K, a pair of peaks at 4126 and 4133 cm^{-1} are observed. Since these peaks only evolve at temperatures significantly lower than those at which occupation of sites I and II initially occurs, they are ascribed to H_2 being weakly adsorbed on the organic scaffold of the framework. As the temperature is lowered further to 14 K, the peak areas of these absorptions increase dramatically, and a third absorption band emerges at 4140 cm^{-1}. The large peak area of these bands compared to that of site I is consistent with the larger crystallographic multiplicity of the weaker adsorption sites within the material.

Fe-BTT. The infrared absorption spectra collected for an H_2-dosed sample of Fe-BTT over a temperature range of 14−150 K are presented in Figure 3c. As the temperature is lowered, a broad absorption band at 3980 cm^{-1} corresponding to H_2 adsorption at site I is observed, and this is the only signal observed above 120 K. The dramatically enhanced shift of this absorption compared to the Mn- (4038) and Cu-BTT (4058 and 4065 cm^{-1}) is consistent with the trend in the zero-coverage isosteric heat of adsorption and the very short Fe^{2+}−D_2 distance of 2.17 Å observed via powder neutron diffraction. In a similar case to the Mn-BTT compound, approximately 30% of the Fe^{2+} cations retain a coordinated MeOH molecule following activation of the material. Consequently, as described above for Mn-BTT (see Figure 3b), this leads to a significant broadening of the infrared absorption band, owing to the presence of multiple binding environments for H_2 arising from a statistical distribution of the coordinated solvent molecules. Upon lowering the temperature below 100 K, a complex group of overlapping bands, originating from the interaction of H_2 with the organic linkers, begins to appear in the 4150−4100 cm^{-1} range and continues to evolve as the temperature is lowered to 14 K.

Enthalpy and Entropy of H_2 Adsorption. The standard enthalpy of adsorption (ΔH_{ads}) for H_2 adsorbed at the primary binding site was probed by generating an Arrhenius-type plot using the peak integrals from the temperature-dependent infrared data for the three compounds (see Figure 4). The magnitudes of the ΔH_{ads} values calculated using this method for Mn-BTT (−11.9 ± 0.6 kJ/mol), Fe-BTT (−12.9 ± 0.3 kJ/mol) and Cu-BTT (−10.4 ± 0.4 kJ/mol) are each comparable to or slightly higher than the corresponding values for the zero-coverage isosteric heats of adsorption in Figure 2. The differences can be ascribed to the fact that the isosteric heat represents the average enthalpy of adsorption across all of the available binding sites, some of which facilitate significantly weaker adsorption than the exposed metal cation site. Nevertheless, the relationship between the magnitudes of the ΔH_{ads} values of the three compounds is consistent with that observed for the isosteric heats of adsorption. The ΔS_{ads} values associated with H_2 adsorption at site I of −68 ± 9 J K^{-1} mol^{-1} for Mn-BTT and Fe-BTT, and −66 ± 9 J K^{-1} mol^{-1} for Cu-BTT is indicative of a greater degree of spatial ordering of the adsorbed H_2 molecules, which leads to a decrease in the number of degrees of freedom for each of the H_2 molecules.

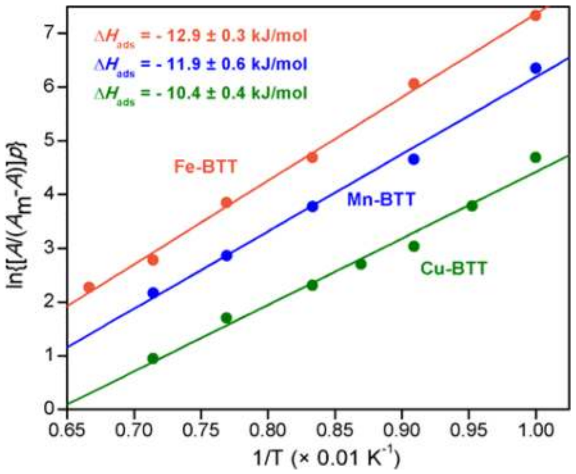

Figure 4. An Arrhenius-type plot derived from the integral of the absorption band corresponding to the exposed cation binding site for Mn- (blue), Fe- (orange), and Cu-BTT (green). The solid lines represent the line of best fit to each set of data.

DFT Calculations. In order to enhance the level of detail in which the thermodynamics of H_2 adsorption within the M-BTT structure type can be described, DFT methods were used as a platform for simulating H_2 binding to sites I and II in the framework. Owing to the extended nature of the network structure, the calculations were performed starting with the model compound $[M_4Cl(tz)_8]^-$ (M = Mn, Cu, Zn; tz^- = 5-H-tetrazolate), for which a sample structure is depicted in Figure 5a. This unit can be considered as a truncated portion of the full structure representing a single tetranuclear metal cluster and its ligand coordination sphere. Here, each of the metal cations is in a square pyramidal environment with a vacant axial coordination site available for H_2 adsorption in the same manner as site I of the full structure. Furthermore, the four tetrazolate units on each side of the metal cluster form a bowl-shaped cavity to simulate the adsorption environment found at site II. Here we model two of the experimentally prepared complexes and expand the theoretical study to include the corresponding Zn-based analog, $[Zn_4Cl(tz)_8]^-$, which can be probed using the present theoretical framework.

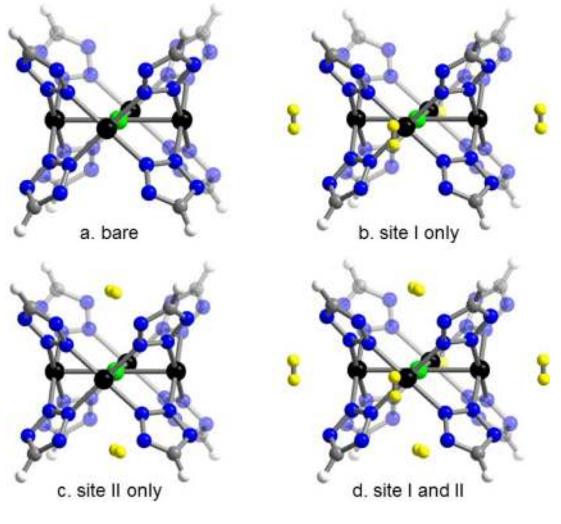
a. bare
b. site I only
c. site II only
d. site I and II

Figure 5. Representative DFT structural models of the hypothetical $[M_4Cl(tz)_8]^-$ (M = Mn, Cu, Zn; tz^- = 5-H-tetrazolate) molecule and its H_2-bound variants calculated for assessment of the H_2 binding energies. For each of the metals surveyed, four structures were calculated. Starting with the parent molecule shown in (a), H_2 molecules were introduced to sites (b) I, (c) II, or (d) I and II. Black, green, white, gray, and blue spheres represent M, Cl, H, C, and N atoms, respectively, while the H atoms of the bound H_2 molecules are displayed as yellow spheres for clarity.

Calculation of Bare Structures. An initial screening of DFT functionals revealed significant deviations in the optimized structural parameters of the initial structures prior to introduction of the adsorbed H_2 molecules. Among these, the bond lengths and angles calculated for $[Mn_4Cl(tz)_8]^-$ and $[Cu_4Cl(tz)_8]^-$ using the ωB97X-D functional correlate most closely with the experimental structures of activated Mn- and Cu-BTT obtained from powder neutron diffraction data, confirming our selection of this functional for studying the H_2-bound structures.

The calculated and experimental bond distances and angles for the three $[(M_4Cl)(tz)_8]^-$ molecules and M-BTT frameworks are presented in Table 1. The ωB97X-D functional provides a close agreement with experiment for the structural parameters for both the Mn- and Cu-based materials. Note that, in the experimental data for Mn-BTT, the relatively large quantity of residual solvent bound to the $[Mn_4Cl]^{7+}$ cluster following activation (MeOH bound to approximately 70% of Mn^{2+} sites) leads to the average position of the Mn^{2+} ion being drawn out of the four-atom mean plane formed by the tetrazolate nitrogens. In contrast, the absence of solvent molecules in the model for $[Mn_4Cl(tz)_8]^-$ results in the optimized coordinates of the Mn^{2+} ions being in a near-idealized square pyramidal coordination environment, wherein the metal centers are essentially within the N_4 plane, providing the maximum degree of interaction with the tetrazolate ligands and the axial chloride ion. Nevertheless, the other theoretical structural parameters agree closely with those obtained experimentally, and the following theoretical results discussed here can be considered representative of an ideal (fully desolvated) case that would be achieved experimentally if improved desolvation conditions are discovered for Mn-BTT. Meanwhile, the ability for the Cu-BTT material to be completely desolvated experimentally provides an opportunity for a more direct comparison of the structural parameters.

Table 1. Comparison of the Structural Parameters Obtained for the Theoretical $[M_4Cl(tz)_8]^-$ (M = Mn, Cu, Zn) Molecules with Experimental Data for Desolvated Mn- and Cu-BTT

	M = Mn		Cu		Zn
	exptl[a]	calcd	exptl[b]	calcd	calcd
			Bond Distance (Å)		
M−Cl	2.798	2.616	2.504	2.456	2.484
M−N(1)	2.217	2.210	2.007	2.040	2.114
N(1)−N(1)	1.261	1.322	1.344	1.323	1.322
N1−N(2)	1.316	1.315	1.323	1.310	1.312
N(2)−C	1.363	1.332	1.354	1.332	1.332
			Bond Angle (°)		
Cl−M−N(1)	82.11	88.77	87.01	89.45	90.13
M−N(1)−N(1)	127.47	122.60	123.18	121.83	121.17
M−N(1)−N(2)	121.67	127.53	127.00	128.15	128.83
N(1)−N(2)−C	105.71	103.87	104.31	103.77	103.76
N(2)−C−N(2)	107.10	112.51	111.69	112.56	112.60

[a]Ref 20. [b]Ref 22.

Indeed, as shown in Table 1, the structure obtained from theory closely reflects that of the experimentally desolvated Cu-BTT structure, highlighting the accuracy of the ωB97X-D functional in accurately describing the metal cluster. In the case of the theoretical $[Zn_4Cl(tz)_8]^-$ molecule, the $[Zn_4Cl]^{7+}$ cluster is slightly contracted compared to the Mn-based analog and exhibits structural parameters similar to the $[Cu_4Cl]^{7+}$ cluster observed within $[Cu_4Cl(tz)_8]^-$. This is consistent with the trend in ionic radii of the three ions, although the isotropic nature of the electron cloud of Zn^{2+} (i.e., the lack of an axial distortion) is expected to provide a higher charge density and consequently a greater adsorption enthalpy compared to Cu^{2+} (see below).

Calculation of H_2-Bound Structures. Following the calculation of the optimized geometries of the bare molecular complexes, H_2 was introduced to simulate the adsorption within the extended solid. As shown in Figure 5b−d, three different cases of H_2 binding were considered, wherein the H_2 was confined to site I or II only (Figure 5b,c, respectively), or allowed to adsorb at both sites (Figure 5d). As shown in Table 2, in a similar manner to the parent molecules, the structural parameters and thermodynamics of H_2 binding were highly dependent on the DFT functional employed. Indeed, among all of the functionals tested, the ωB97X-D functional resulted in site I binding energies and M−H_2 distances (M = Mn, Cu) closest to those obtained experimentally, providing further confirmation of its high accuracy in describing this structure type.

Table 2. HBE (kJ/mol) and M−H_2 Distances (Å) at the Exposed Metal Cation (site I) for $[(M_4Cl)(tz)_8]^-$ (M = Mn, Cu, Zn) as Calculated Using Different DFT Functionals[a]

	M = Mn		Cu		Zn	
functional	HBE (kJ/mol)	M−H_2 (Å)	HBE (kJ/mol)	M−H_2 (Å)	HBE (kJ/mol)	M−H_2 (Å)
LDA	−29.4	2.14	−20.3	2.22	−30.6	2.07
BLYP	−0.8	2.51	1.3	3.87	0.7	2.61
BP86	−3.0	2.39	1.7	4.61	−1.8	2.33
PBE	−8.8	2.37	−2.8	2.75	−7.5	2.33
B3LYP	−5.0	2.42	−0.1	2.93	−3.2	2.40
ωB97	−25.4	2.25	−14.5	2.43	−21.7	2.24
ωB97X	−22.0	2.29	−13.0	2.46	−19.2	2.26
ωB97X−D	−17.2	2.32	−10.8	2.49	−16.3	2.27
exptl	−11.9	2.23	−10.4	2.47	−	−

[a] All HBE values corrected using BSSE and ZPE from ωB97X-D calculations.

A closer inspection of the results for the H_2-bound complexes reveals a relatively large difference in the adsorption energies between sites I and II (see Table 3). The difference is particularly large in the Mn case, for which site I exhibits a H_2 binding energy of −17.2 kJ/mol, compared to just −7.5 kJ/mol for site II. The binding strengths of the two sites are significantly closer in energy in the Cu-based model, which is supported by previous neutron diffraction data in which both sites I and II are populated at similar occupancies even for the lowest guest loadings. As expected, despite the similar structural parameters of $[Cu_4Cl(tz)_8]^-$ and $[Zn_4Cl(tz)_8]^-$, the latter exhibits a considerably higher binding energy. In fact, in the case where H_2 was allowed to populate both sites I and II, the Zn compound showed the most promise for binding hydrogen, displaying a slightly greater overall affinity for H_2 than $[Mn_4Cl(tz)_8]^-$. This high affinity is further reflected in the M−H_2 distances, in which $[Zn_4Cl(tz)_8]^-$ displayed the shortest calculated distance out of the compounds studied. Meanwhile, the Cl···H_2 distances are essentially invariant with the identity of the metal, which is consistent with the calculated site II H_2 binding energies of approximately −7 kJ/mol for each of the three compounds.

Table 3. Comparison of the Structural and Thermodynamic Parameters Obtained Using the ωB97X-D Functional for $[M_4Cl(tz)_8]^-$ (M = Mn, Cu, Zn) Molecules with Experimental Data for Desolvated Mn- and Cu-BTT

		M = Mn		Cu		Zn
		calcd	exptl	calcd	exptl	calcd
HBE (kJ/mol)	site I only	−17.2	−11.9[a]	−10.8	−10.4[a]	−16.3
	site II only	−7.5		−7.0		−7.7
	site I + II	−13.6	−10.6[b]	−10.1	−9.8[b]	−14.1
H_2 distance (Å)	M−H_2 (site I)	2.33	2.27[c]	2.56	2.47[c]	2.27
	Cl···H_2 (site II)	3.25	3.47[c]	3.20	3.46[c]	3.22
Δν (cm^{-1})	site I	−125	−123[a]	−78	−100[a]	−129
	site II	−16	−31[a]	−14	−41[a]	−16

[a] Based on infrared data. [b] Zero-coverage isosteric heat of adsorption. [c] Based on neutron diffraction data.

The change in the vibrational frequency for H_2 bound at each of the adsorption sites is also presented in Table 3. For each of the three systems, the frequency for H_2 bound at site I is red-shifted by a greater amount than the molecules adsorbed at site II. The degree of the shift is also found to correlate with the adsorption energy, with H_2 bound at site I within the Mn- and Zn-based molecules being shifted by −125 and −129 cm^{-1} from the vibrational frequency of free H_2, while the corresponding value is shifted by just −78 cm^{-1} in the Cu case. The shifts are in general within 20 cm^{-1} of the values observed experimentally, which are sufficiently accurate to support the original assignments made in the discussion of the infrared spectra above.

Effect of Anion Substitution on H_2 Adsorption. Using the hypothetical $[(Zn_4Cl)_3(tz)_8]^-$ as a platform for further study, the effect of substitution of the central anion within the tetranuclear cluster was probed in the context of H_2 adsorption. Here, the Cl^- anion was substituted with F^- and Br^-, and a vacant case as observed within the cluster of the structurally related compound $Ni_3(BTP)_2$ (BTP^{3-} = 1,3,5-benzenetrispyrazolate)[31] was also investigated. The substituted clusters are depicted in Figure 6, and the related structural and thermodynamic data are presented in Table 4. As can be seen in the structures, the size of the anion plays a vital role in the position of the metal centers. For the smallest anion (F^-), the comparatively short Zn−F bond of 2.352 Å results in the metal ions being located beneath the four-atom mean plane of the tetrazolate nitrogen atoms, as indicated by the F−Zn−N angle of 92.3° (note that a Zn atom that lies exactly in the nitrogen plane would exhibit an angle of 90°). In contrast, when the size of the anion is increased to Br^-, the longer Zn−Br bond of 2.561 Å leads to the Zn^{2+} ions being positioned slightly out of the N_4 plane. In the case of a vacancy at the center of the cluster, the metal centers are projected considerably out of the plane, presumably in order to minimize the repulsive force between positive charges. Indeed, such a displacement of the metal center has been experimentally observed in the case of $Ni_3(BTP)_2$. Interestingly, the site I H_2 binding energies calculated for the four clusters is highest in the

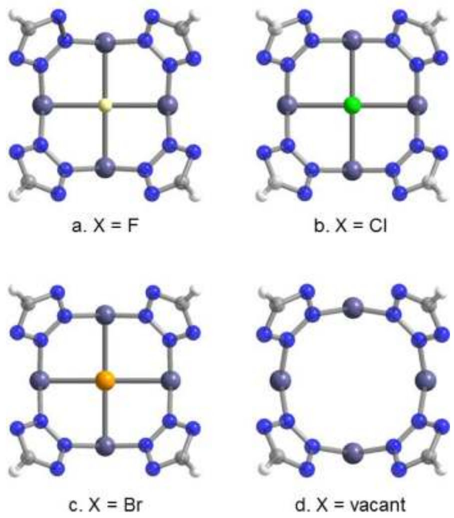
a. X = F b. X = Cl

c. X = Br d. X = vacant

Figure 6. Molecular structures as calculated using the ωB97X-D functional for $[(Zn_4X)(tz)_8]^-$, where X = (a) F, (b) Cl, (c) Br, and of (d) $[Zn_4(tz)_8]$, in which the center of the cluster is vacant. Light-purple, yellow, green, orange, white, gray, and blue spheres represent Zn, F, Cl, Br, H, C, and N atoms, respectively. Bound H_2 molecules have been omitted for clarity.

Table 4. HBE (kJ/mol) and M−H_2 Distances (Å) at the Exposed Metal Cation (site I) for $[(Zn_4X)(tz)_8]^-$ As Calculated Using the ωB97X-D Functional[a]

X^-	Zn−X (Å)	X−Zn−N (°)	Zn−H_2 (Å)	HBE (kJ/mol)
F^-	2.352	92.3	2.394	−13.4
Cl^-	2.509	89.6	2.268	−16.3
Br^-	2.561	89.0	2.235	−17.3
vacant	2.669[b]	83.8[b]	2.075	−25.7

[a] HBE values corrected using BSSE and ZPE from the chloride calculations. [b] Calculated by placing a centroid at the center of the tetranuclear cluster.

case of the vacancy, and weakest for X = F^-. This is in contrast to what may be predicted from the perspective of electronegativity, in which the more electron-withdrawing F^- ion might be expected to promote a more positive partial charge on the Zn^{2+} ions, leading to a more polarizing binding environment at site I. The calculations presented here suggest that the projection of the metal centers out of the nitrogen plane results in a more readily accessible binding site, allowing the adsorbing H_2 molecules to interact more strongly with its positive charge. Moreover, from the perspective of increasing the enthalpy of adsorption at site I, the use of more diffuse counteranions is expected to lead to stronger M−H_2 interactions, which are vital to improving the overall H_2 storage properties.

■ CONCLUSION

The foregoing results demonstrate the success of a complementary experimental and theoretical approach in obtaining a complete picture of the H_2 adsorption properties within the M-BTT structure type. Indeed, the judicious selection of the most appropriate DFT functional has allowed several unknown systems to be analyzed, allowing the Zn-based framework, Zn-BTT, to be identified as a potential synthetic target for further study. Moreover, the anion has been demonstrated as playing a crucial role in determining the H_2 binding energy, and more diffuse anions that project the metal ions away from the center of the cluster appear to provide more benefit than highly electronegative ions. Efforts are currently underway to synthesize the Zn-based analog, other M-BTT frameworks containing other anions at the center of the metal clusters, as well as the preparation of new materials derived from high-valent (e.g., trivalent or tetravalent) metal ions, which may provide a further enhancement in the enthalpy of adsorption of H_2.

■ ASSOCIATED CONTENT

Ⓢ Supporting Information

Adsorption isotherms, additional information regarding the dual-site Langmuir fits to the isotherm data, and desorption infrared data (PDF). This material is available free of charge via the Internet at http://pubs.acs.org.

■ AUTHOR INFORMATION

Corresponding Author

silvia.bordiga@unito.it; mhg@cchem.berkeley.edu; jrlong@berkeley.edu

Present Addresses

[⊥] Department of Physics, Center for Theoretical Sciences, and Center for Quantum Science and Engineering, National Taiwan University, Taipei 10617, Taiwan
[∇] Institute for Energy Technology, Instituttveien 18, P.O. Box 40, N-2027, Kjeller, Norway
[#] Department of Chemistry, Center for Catalysis, University of Florida, Gainesville, Florida 32611, United States
[○] Department of Chemistry, Massachusetts Institute of Technology, Cambridge, Massachusetts 02139, United States

Author Contributions

[◆] These authors contributed equally to this work.

Notes

The authors declare no competing financial interest.

■ ACKNOWLEDGMENTS

This research was funded by the United States Department of Energy, Energy Efficiency and Renewable Energy, Hydrogen and Fuel Cell Program. The work in Torino was funded by Ateneo-Compagnia di San Paolo-2011- 1A line, OR-TO11RRT5 project. We thank Fulbright New Zealand for partial support of K.S. and Dr. C. M. Brown and Mr. J. A. Mason for helpful discussions.

■ REFERENCES

(1) (a) Metz, B.; Davidson, O.; de Coninck, H.; Loos, M.; Meyer, L. *Special Report on Carbon Dioxide Capture and Storage*; Cambridge University Press: Cambridge, 2005. (b) Chu, S. *Science* **2009**, *325*, 1599. (c) Haszeldine, R. S. *Science* **2009**, *325*, 1647.

(2) Schlapbach, L.; Züttel, A. *Nature* **2001**, *414*, 353.

(3) *EERE: Hydrogen, Fuel Cells, and Infrastructure Technologies Program*; U.S. Department of Energy: Washington, D.C.; http://www.eere.energy.gov/hydrogenandfuelcells, (accessed August, 2012).

(4) (a) Aceves, S. M.; Berry, G. D.; Martinez-Frias, J.; Espinosa-Loza, F. *Int. J. Hydrogen Storage* **2006**, *31*, 2274. (b) Kumar, V. S.; Raghunathan, K.; Kumar, S. *Int. J. Hydrogen Storage* **2009**, *34*, 5466.

(5) Sakituna, B.; Lamari-Darkrim, F.; Hirscher, M. *Int. J. Hydrogen Energy* **2007**, *32*, 1121.

(6) (a) Dincă, M.; Long, J. R. *Angew. Chem., Int. Ed.* **2008**, *47*, 6766. (b) Murray, L. J.; Dincă, M.; Long, J. R. *Chem. Soc. Rev.* **2009**, *38*, 1294. (c) Sculley, J.; Yuan, D.; Zhou, H.-C. *Energy Environ. Sci.* **2011**, *4*, 2721. (d) Getman, R. B.; Bae, Y.-S.; Wilmer, C. E.; Snurr, R. Q.

2012, *112*, 782. (e) Suh, M. P.; Park, H. J.; Prasad, T. H.; Lim, D.-W. *Chem. Rev.* **2012**, *112*, 782.

(7) Bhatia, S. K.; Myers, A. L. *Langmuir* **2006**, *22*, 1688.

(8) (a) Garrone, E.; Bonelli, B.; Otero Areán, C. *Chem. Phys. Lett.* **2008**, *456*, 68. (b) Otero Areán, C.; Chavan, S.; Cabello, C. P.; Garrone, E.; Palomino, G. T. *ChemPhysChem* **2010**, *11*, 3237.

(9) (a) Eddaoudi, M.; Kim, J.; Rosi, N.; Vodak, D.; Wachter, J.; O'Keeffe, M.; Yaghi, O. M. *Science* **2002**, *295*, 469. (b) Matsuda, R.; Kitaura, R.; Kitagawa, S.; Kubota, Y.; Belosludov, R. V.; Kobayashi, T. C.; Sakamoto, H.; Chiba, T.; Takata, M.; Kawazoe, Y.; Mita, Y. *Nature* **2005**, *436*, 238. (c) Millward, A. R.; Yaghi, O. M. *J. Am. Chem. Soc.* **2005**, *127*, 17998. (d) Furukawa, H.; Miller, M. A.; Yaghi, O. M. *J. Mater. Chem.* **2007**, *17*, 3197. (e) Ma, S.; Sun, D.; Simmons, J. M.; Collier, C. D.; Yuan, D.; Zhou, H. C. *J. Am. Chem. Soc.* **2008**, *130*, 1012. (f) Morris, R. E.; Wheatley, P. S. *Angew. Chem., Int. Ed.* **2008**, *47*, 4966. (g) Llewellyn, P. L.; Bourrelly, S.; Serre, C.; Vimont, A.; Daturi, M.; Hamon, L.; De Weireld, G.; Chang, J.-S.; Hong, D.-Y.; Hwang, Y. K.; Jhung, S. H.; Férey, G. *Langmuir* **2008**, *24*, 7245. (h) Furukawa, H.; Ko, N.; Go, Y. B.; Aratani, N.; Choi, S. B.; Choi, E.; Yazaydin, A. Ö; Snurr, R. Q.; O'Keeffe, M.; Kim, J.; Yaghi, O. M. *Science* **2010**, *329*, 424.

(10) (a) Rosi, N. L.; Eckert, J.; Eddaoudi, M.; Vodak, D. T.; Kim, J.; O'Keeffe, M.; Yaghi, O. M. *Science* **2003**, *300*, 1127. (b) Férey, G.; Latroche, M.; Serre, C.; Millange, F.; Loiseau, T.; Percheron-Guégan, A. *Chem. Commun.* **2003**, 2976. (c) Rowsell, J. L.; Millward, A. R.; Park, K. S.; Yaghi, O. M. *J. Am. Chem. Soc.* **2004**, *126*, 5666. (d) Lee, E. Y.; Suh, M. P. *Angew. Chem., Int. Ed.* **2004**, *43*, 2798. (e) Sun, D.; Ma, S.; Ke, Y.; Collins, D. J.; Zhou, H.-C. *J. Am. Chem. Soc.* **2006**, *128*, 3896. (f) Rowsell, J. L. C.; Yaghi, O. M. *J. Am. Chem. Soc.* **2006**, *128*, 1304. (g) Wong-Foy, A. G.; Matzger, A. J.; Yaghi, O. M. *J. Am. Chem. Soc.* **2006**, *128*, 3494. (h) Lin, X.; Jia, J.; Zhao, X.; Thomas, K. M.; Blake, A. J.; Walker, G. S.; Champness, N. R.; Hubberstey, P.; Schröder, M. *Angew. Chem., Int. Ed.* **2006**, *45*, 7358. (i) Latroche, M.; Surblé, S.; Serre, C.; Mellot-Draznieks, C.; Llewellyn, P. L.; Lee, J.-H.; Chang, J.-S.; Jhung, S. H.; Férey, G. *Angew. Chem., Int. Ed.* **2006**, *45*, 8227. (j) Xiao, B.; Wheatley, P. S.; Zhao, X.; Fletcher, A. J.; Fox, S.; Rossi, A. G.; Megson, I. L.; Bordiga, S.; Regli, L.; Thomas, K. M.; Morris, R. E. *J. Am. Chem. Soc.* **2007**, *129*, 1203. (k) Furukawa, H.; Miller, M. A.; Yaghi, O. M. *J. Mater. Chem.* **2007**, *17*, 3197. (l) Kaye, S. S.; Dailly, A.; Yaghi, O. M.; Long, J. R. *J. Am. Chem. Soc.* **2007**, *129*, 14176. (m) Koh, K.; Wong-Foy, A. G.; Matzger, A. J. *J. Am. Chem. Soc.* **2009**, *131*, 4184. (n) Sumida, K.; Hill, M. R.; Horike, S.; Dailly, A.; Long, J. R. *J. Am. Chem. Soc.* **2009**, *131*, 15120. (o) Farha, O. K.; Yazaydin, A. O.; Eryazici, I.; Malliakas, C. D.; Hauser, B. G.; Kanatzidis, M. G.; Nguyen, S. T.; Snurr, R. Q.; Hupp, J. T. *Nat. Chem.* **2010**, *2*, 944. (p) Park, H. J.; Lim, D.-W.; Yang, W. S.; Oh, T.-R.; Suh, M. P. *Chem, Eur. J.* **2011**, *17*, 7251. (q) Liu, D.; Wu, H.; Wang, S.; Xie, Z.; Li, J.; Lin, W. *Chem. Sci.* **2012**, *3*, 3032. (r) Tranchemontagne, D. J.; Park, K. S.; Furukawa, H.; Eckert, J.; Knobler, C. B.; Yaghi, O. M. *J. Phys. Chem. C* **2012**, *116*, 13143.

(11) (a) Dietzel, P. D. C.; Morita, Y.; Blom, R.; Fjellvag, H. *Angew. Chem., Int. Ed.* **2005**, *44*, 6354. (b) Dincă, M.; Long, J. R. *J. Am. Chem. Soc.* **2005**, *127*, 9376. (c) Rosi, N. L.; Kim, J.; Eddaoudi, M.; Chen, B.; O'Keeffe, M.; Yaghi, O. M. *J. Am. Chem. Soc.* **2005**, *127*, 1504. (d) Vimont, A.; Goupil, J.-M.; Lavalley, J.-C.; Daturi, M.; Surblé, S.; Serre, C.; Millange, F.; Férey, G.; Audebrand, N. *J. Am. Chem. Soc.* **2006**, *128*, 3218. (e) Moon, H. R.; Kobayashi, N.; Suh, M. P. *Inorg. Chem.* **2006**, *45*, 8672. (f) Dietzel, P. D. C.; Panella, B.; Hirscher, M.; Blom, R.; Fjellvag, H. *Chem. Commun.* **2006**, 959. (g) Caskey, S. R.; Wong-Foy, A. G.; Matzger, A. J. *J. Am. Chem. Soc.* **2008**, *130*, 10870. (h) Dietzel, P. D. C.; Blom, R.; Fjellvag, H. *Eur. J. Inorg. Chem.* **2008**, 3624. (i) Liu, Y.; Kabbour, H.; Brown, C. M.; Neumann, D. A.; Ahn, C. C. *Langmuir* **2008**, *24*, 4772. (j) Zhou, W.; Wu, H.; Yildirim, T. *J. Am. Chem. Soc.* **2008**, *130*, 15268. (k) Dietzel, P. D. C.; Besikiotis, V.; Blom, R. *J. Mater. Chem.* **2009**, *19*, 7362. (l) Cheon, Y. E.; Suh, M. P. *Chem. Commun.* **2009**, 2296. (m) Yuan, D.; Zhao, D.; Sun, D.; Zhou, H.-C. *Angew. Chem., Int. Ed.* **2010**, *49*, 5357. (n) Yan, Y.; Blake, A. J.; Lewis, W.; Barnett, S. A.; Dailly, A.; Champness, N. R.; Schröder, M. *Chem.—Eur. J.* **2011**, *17*, 11162. (o) Sumida, K.; Brown, C. M.; Herm, Z. R.; Chavan, S.; Bordiga, S.; Long, J. R. *Chem. Commun.* **2011**, *50*, 1157. (p) Sumida, K.; Her, J.-H.; Dincă, M.; Murray, L. J.; Schloss, J. M.; Pierce, C. J.; Thompson, B. A.; FitzGerald, S. A.; Brown, C. M.; Long, J. R. *J. Phys. Chem. C* **2011**, *115*, 8414.

(12) Vitillo, J. G.; Gegli, L.; Chavan, S.; Ricchiardi, G.; Spoto, G.; Dietzel, P. D. C.; Bordiga, S.; Zecchina, A. *J. Am. Chem. Soc.* **2008**, *130*, 8386.

(13) Parr, R. G.; Yang, W. *Density-Functional Theory of Atoms and Molecules*; Oxford University Press: New York, 1989.

(14) Kohn, W.; Becke, A. D.; Parr, R. G. *J. Phys. Chem.* **1996**, *100*, 12974.

(15) (a) Kristyán, S.; Pulay, P. *Chem. Phys. Lett.* **1994**, *229*, 175. (b) Perdew, J. P. *Phys. Rev. B* **1981**, *23*, 5048. (c) Dutoi, A. D.; Head-Gordon, M. *Chem. Phys. Lett.* **2006**, *422*, 230.

(16) Wu, X.; Vargas, M. C.; Nayak, S.; Lotrich, V.; Scoles, G. *J. Chem. Phys.* **2001**, *115*, 8748.

(17) Wu, Q.; Yang, W. *J. Chem. Phys.* **2002**, *116*, 515.

(18) Chai, J.-D.; Head-Gordon, M. *Phys. Chem. Chem. Phys.* **2008**, *10*, 6615.

(19) Goerigk, L.; Grimme, S. *Phys. Chem. Chem. Phys.* **2011**, *13*, 6670.

(20) Dincă, M.; Dailly, A.; Liu, Y.; Brown, C. M.; Neumann, D. A.; Long, J. R. *J. Am. Chem. Soc.* **2006**, *128*, 16876.

(21) Sumida, K.; Horike, S.; Kaye, S. S.; Herm, Z. R.; Queen, W. L; Brown, C. M.; Grandjean, F.; Long, G. J.; Dailly, A.; Long, J. R. *Chem. Sci.* **2010**, *1*, 184.

(22) Dincă, M.; Han, W. S.; Liu, Y.; Dailly, A.; Brown, C. M.; Long, J. R. *Angew Chem., Int. Ed.* **2007**, *46*, 1419.

(23) Note that two other M-BTT analogs have been reported recently; $[Co(DMA)_6]_3[(Co_4Cl)_3(BTT)_8(H_2O)_{12}]_2 \cdot 12H_2O$ (solvated Co-BTT) and $[Cd(DMF)_6]_3[(Cd_4Cl)_3(BTT)_8(H_2O)_{12}]_2 \cdot 14H_2O \cdot 4DMF$ (solvated Cd-BTT): Biswas, S.; Maes, M.; Dhakshinamoorthy, A.; Feyand, M.; De Vos, D. E.; Garcia, H.; Stock, N. *J. Mater. Chem.* **2012**, *22*, 10200.

(24) Mason, J. A.; Sumida, K.; Herm, Z. R.; Krishna, R.; Long, J. R. *Energy Environ. Sci.* **2011**, *4*, 3030.

(25) Shao., Y.; et al. *Phys. Chem. Chem. Phys.* **2006**, *8*, 3172.

(26) Krishnan, R.; Binkley, J. S.; Seeger, R.; Pople, J. A. *J. Chem. Phys.* **1980**, *72*, 650.

(27) McLean, A. D.; Chandler, G. S. *J. Chem. Phys.* **1980**, *72*, 5639.

(28) Dolg, M.; Wedig, U.; Stoll, H.; Preuss, H. *J. Chem. Phys.* **1987**, *86*, 2123.

(29) Boys, S.; Bernardi, F. *Mol. Phys.* **1970**, *19*, 553.

(30) Lamberti, C.; Zecchina, A.; Groppo, E.; Bordiga, S. *Chem. Soc. Rev.* **2010**, *39*, 4951.

(31) Colombo, V.; Galli, S.; Choi, H. J.; Han, G. D.; Maspero, A.; Palmisano, G.; Masciocchi, N.; Long, J. R. *Chem. Sci.* **2011**, *2*, 1311.